Response of Northern Hemisphere Midlatitude Circulation to Arctic Amplification in a Simple Atmospheric General Circulation Model

YUTIAN WU

Department of Earth, Atmospheric, and Planetary Sciences, Purdue University, West Lafayette, Indiana

KAREN L. SMITH

Lamont-Doherty Earth Observatory, Columbia University, Palisades, New York

(Manuscript received 24 August 2015, in final form 8 December 2015)

ABSTRACT

This study examines the Northern Hemisphere midlatitude circulation response to Arctic amplification (AA) in a simple atmospheric general circulation model. It is found that, in response to AA, the tropospheric jet shifts equatorward and the stratospheric polar vortex weakens, robustly for various AA forcing strengths. Despite this, no statistically significant change in the frequency of sudden stratospheric warming events is identified. In addition, in order to quantitatively assess the role of stratosphere–troposphere coupling, the tropospheric pathway is isolated by nudging the stratospheric zonal mean state toward the reference state. When the nudging is applied, rendering the stratosphere inactive, the tropospheric jet still shifts equatorward but by approximately half the magnitude compared to that of an active stratosphere. The difference represents the stratospheric pathway and the downward influence of the stratosphere on the troposphere. This suggests that stratosphere–troposphere coupling plays a nonnegligible role in establishing the midlatitude circulation response to AA.

1. Introduction

The Arctic has experienced a large near-surface warming trend during the past few decades, about twice as large as the global average, and this is widely known as Arctic amplification (AA). As a consequence of increasing anthropogenic greenhouse gases, state-of-the-art climate models have consistently suggested a further warming of the Arctic, which is again about 2 times the global average warming in the annual mean at the end of the twenty-first century (see Collins et al. 2013). Projected AA peaks in early winter (November–December) and has a consistent vertical structure that exhibits the largest warming near the surface extending to the midtroposphere. It is likely that AA is caused by a mixture of mechanisms, not only limited to sea ice and snow albedo feedback but also including longwave radiation feedback, lapse rate feedback, increased moisture transport, and increased oceanic transport [see references in Collins et al. (2013) and Pithan and Mauritsen (2014)].

There is an increasing body of observational and modeling evidence that AA might strongly impact both the weather and climate, not only in the Arctic region but also remotely in the Northern Hemisphere (NH) midlatitudes [see review articles by Cohen et al. (2014) and Barnes and Screen (2015) and references therein]. In general, most of these studies have detected an atmospheric circulation response resembling a negative North Atlantic Oscillation (NAO) or northern annular mode (NAM) pattern as a result of sea ice decline and accompanied AA. However, discrepancies in the atmospheric circulation response exist among different model integrations. For example, Screen et al. (2013) used two independent atmospheric general circulation models (AGCMs) forced with identical sea ice loss and found large disagreement on the timing and magnitude of the response.

The adjustment of atmospheric circulation to sea ice loss has been studied extensively, with the primary focus on the tropospheric pathway. It was found that transient eddy feedbacks play an important role in shaping the

Corresponding author address: Yutian Wu, Department of Earth, Atmospheric, and Planetary Sciences, Purdue University, 550 Stadium Mall Dr., West Lafayette, IN 47907.
E-mail: wu640@purdue.edu

DOI: 10.1175/JCLI-D-15-0602.1

© 2016 American Meteorological Society

circulation response in equilibrium and that they significantly contribute to the transition from the initial baroclinic response to an equivalent barotropic response with enhanced magnitude and spatial extent [e.g., Deser et al. (2004) and references therein]. Besides the tropospheric pathway, Cohen et al. (2014) and Barnes and Screen (2015) suggested that a stratospheric pathway may also be an important mechanism by which AA could modify the midlatitude circulation. The stratospheric pathway has received greater attention lately yet is not fully understood. An example of the stratospheric pathway linking cryospheric variability and the NAM is the observed and simulated connection between October Eurasian snow cover and midlatitude surface weather conditions in winter (Cohen et al. 2007; Fletcher et al. 2009; Cohen et al. 2010; Smith et al. 2010). The mechanism involves a two-way stratosphere–troposphere interaction: a snow-forced planetary wave anomaly propagates upward from the troposphere into the stratosphere, primarily as a result of linear constructive interference (when the wave anomaly is in phase with the climatology), and drives a weakening of the stratospheric polar vortex. The stratospheric circulation anomaly later propagates downward back into the troposphere after weeks to months, resulting in a negative NAM pattern near the surface. As a consequence of AA and the possible increase in planetary-scale wave activity (e.g., Peings and Magnusdottir 2014; Feldstein and Lee 2014; Kim et al. 2014; Sun et al. 2015), we expect a similar stratosphere–troposphere coupling to connect AA with the NH midlatitude circulation anomalies. However, previous studies do not even agree on the stratospheric circulation response—some modeling studies reported a strengthened stratospheric polar vortex (e.g., Scinocca et al. 2009; Cai et al. 2012; Screen et al. 2013; Sun et al. 2014), whereas others found a weakening (e.g., Peings and Magnusdottir 2014; Feldstein and Lee 2014; Kim et al. 2014) followed by a negative NAM anomaly in the troposphere and near the surface.

In particular, recent studies of Sun et al. (2014, 2015) conducted identical prescribed sea ice loss experiments with a pair of low-top (poorly resolved stratosphere) and high-top (well-resolved stratosphere) AGCMs: Community Atmosphere Model, version 4 (CAM4), and Whole Atmosphere Community Climate Model, version 4 (WACCM4). Both CAM4 and WACCM4 are developed at the National Center for Atmospheric Research (NCAR) and have identical horizontal resolution and physics (except for the gravity wave and surface wind stress parameterizations); however, their vertical extents are vastly different (~45 versus ~140 km). Sun et al. (2014, 2015) found that the negative NAM response in the troposphere in WACCM4 is qualitatively similar to that in CAM4 but is statistically significantly stronger. The difference between WACCM4 and CAM4 appears as a downward-migrating signal from the stratosphere to the troposphere. However, because of several other factors that may play a role, such as different climatological mean states between the low-top and high-top models, Sun et al. (2014, 2015) could not make a definite conclusion on the importance of the stratospheric pathway. In addition, Sun et al. (2015) explicitly demonstrated that the stratospheric circulation response could be sensitive to the geographical locations of Arctic sea ice loss. When the AGCM was forced with the sea ice loss within the Arctic Circle, mostly over the Barents and Kara Seas (B-K Seas), the circulation showed a weakening of the stratospheric polar vortex. However, a strengthened polar vortex was found with prescribed sea ice loss outside the Arctic Circle, largely over the Pacific Ocean.

In this study, we investigate the response of NH midlatitude circulation to AA in an idealized dry AGCM. In particular, we aim to address two key questions:

1) What is the robust response in the troposphere and stratosphere to AA?
2) What is the role of stratosphere–troposphere coupling in driving the midlatitude circulation response to AA?

The idealized dry AGCM largely isolates the dynamics from uncertainties arising from complex physical parameterizations, and a thorough but computationally affordable exploration of parameter sensitivities can be performed. More importantly, the idealized model allows for an explicit separation of tropospheric and stratospheric pathway, which may not be easily accomplished in comprehensive AGCMs.

This paper is organized as follows. In section 2 we describe the model setup, numerical experiments, and diagnostic methods used in this study. In section 3 we analyze the response in the troposphere and stratosphere to AA and the role of stratosphere–troposphere coupling. A discussion and conclusions in section 4 concludes the paper.

2. Model experiments and methods

a. Model setup

We use a simplified AGCM as described in Smith et al. (2010, hereafter SFK10). The model has a dry dynamical core developed by the Geophysical Fluid Dynamics Laboratory that integrates the primitive equations driven by idealized physics (Held and Suarez 1994). The temperature field is linearly relaxed to an analytical radiative equilibrium temperature profile T_{eq}

that is zonally symmetric. The asymmetry of the temperature profile between the two hemispheres is denoted by ϵ. For a simple representation of stratospheric conditions, the relaxation temperature is modified to include a polar vortex, the strength of which is determined by a temperature lapse rate γ (Polvani and Kushner 2002). Following SFK10, the model configuration used here consists of $\gamma = 2\,\mathrm{K\,km^{-1}}$ and $\epsilon = 10$ for NH perpetual winter conditions. The model also uses realistic topography that allows for the excitation of a rather realistic planetary-scale stationary wave pattern. We integrate the model for 20 000 days at spectral T42 horizontal resolution with 40 levels in the vertical and a model top at 0.02 hPa.

The primary reason we choose the SFK10 model version for our study is that this model has a reasonable representation of the stratosphere and its variability. As will be demonstrated in section 3, the maximal strength of the polar vortex at 10 hPa is about $30\,\mathrm{m\,s^{-1}}$, and the frequency of sudden stratospheric warmings (SSWs) is about 0.27 per 100 days (smaller than observed, to be discussed later). More importantly, this model version has a tropospheric jet located near 40°N, which is close to observed circulation in NH winter.

Despite simulating the opposite-signed response compared to observations and comprehensive GCM simulations, SFK10 successfully used this model to understand the dynamical mechanisms underlying the wintertime NAM driven by autumn snow cover anomalies over Siberia. They found that the model was able to successfully capture the troposphere–stratosphere coupling. The anomalous autumn snow cover and resulting regional surface cooling generates a planetary-scale wave anomaly that is in phase with the climatology, and as a result of constructive interference, the upward-propagating wave anomaly into the stratosphere is further amplified, leading to a weakening of the stratospheric polar vortex. This NAM anomaly migrates downward into the troposphere and affects the surface weather in the subsequent winter (Fletcher et al. 2009).

b. Numerical experiments

To isolate the effect of AA, we follow the methodology of Butler et al. (2010) and add a simple AA-like thermal forcing, maximized at the northern polar surface, to the temperature equation:

$$\frac{\partial T}{\partial t} = \cdots - \kappa_T(\phi,\sigma)\{T - [T_{\mathrm{eq}}(\phi,\sigma) + T_{\mathrm{eq}}^{\mathrm{AA}}(\phi,\sigma)]\}, \quad (1)$$

where κ_T is the Newtonian relaxation time and T_{eq}, as a function of latitude ϕ and sigma level σ, is the original radiative equilibrium temperature profile in SFK10 that includes a stratospheric polar vortex. The perturbation $T_{\mathrm{eq}}^{\mathrm{AA}}$ is designed to mimic AA and can be written as follows:

$$T_{\mathrm{eq}}^{\mathrm{AA}}(\phi,\sigma) = \begin{cases} T_0^{\mathrm{AA}} \cos^k(\phi - 90°) e^{m(\sigma-1)}, & \text{for} \quad \phi > 0 \\ 0, & \text{for} \quad \phi \le 0 \end{cases}, \quad (2)$$

where T_0^{AA} is the perturbation magnitude and k and m are parameters that determine the latitudinal and vertical extent of the warming perturbation, respectively. This analytical formula of $T_{\mathrm{eq}}^{\mathrm{AA}}$ is adopted from Butler et al. (2010), who examined the scenario with $k = 15$, $m = 6$, and the maximum heating rate is $0.5\,\mathrm{K\,day^{-1}}$ (which is approximately equivalent to $T_0^{\mathrm{AA}} = 20\,\mathrm{K}$, assuming a relaxation time scale of 40 days) and found an equatorward shift of the tropospheric jet.

Here we derive $T_{\mathrm{eq}}^{\mathrm{AA}}$ from the projected zonal-mean temperature response during 2080–99 in the representative concentration pathway 8.5 (RCP8.5) scenario, compared to 1980–99 in the historical scenario, averaged across 30 models participating in phase 5 of the Coupled Model Intercomparison Project (CMIP5). Figure 1 shows the zonal-mean temperature response averaged over November–December, the season of maximum AA in CMIP5 multimodel averages. It comprises a large tropical upper-tropospheric warming and an even larger NH AA as well as stratospheric cooling. It is worth noticing that the projected AA not only concentrates near the surface but also extends to the midtroposphere. We fit the CMIP5 temperature response with the $T_{\mathrm{eq}}^{\mathrm{AA}}$ in Eq. (2) with $T_0^{\mathrm{AA}} = 15\,\mathrm{K}$, $k = 5$, and $m = 3$. To investigate the sensitivity of the circulation response to the forcing, we vary T_0^{AA} over a range of forcing strengths (i.e., $T_0^{\mathrm{AA}} = 5$, 10, 15, 20, and 25 K) while fixing the meridional and vertical extent of the forcing (i.e., $k = 5$ and $m = 3$). The control experiment in the absence of AA is denoted by CTRL, and the sensitivity experiments with imposed AA-like forcings are denoted by AA5, AA10, AA15, AA20, and AA25 for the range of forcing strengths.

We emphasize here that our study of AA is different from some previous studies in that it is not limited to the effect of Arctic sea ice loss. Instead we focus on the rather deep and wide warming at northern high latitudes, and as shown in Fig. 1, the 5-K warming extends to about 50°N and 600 hPa. As discussed previously, this feature of AA is likely due to many factors such as longwave radiation feedback, lapse rate feedback, increased moisture transport, and increased oceanic transport [see references in Collins et al. (2013) and Pithan and Mauritsen (2014)].

In addition, in order to separate the tropospheric and stratospheric pathway, we make use of a nudging method as in Simpson et al. (2011, 2013). To isolate the tropospheric circulation response to AA via the tropospheric pathway only, the zonal-mean (wave 0) vorticity,

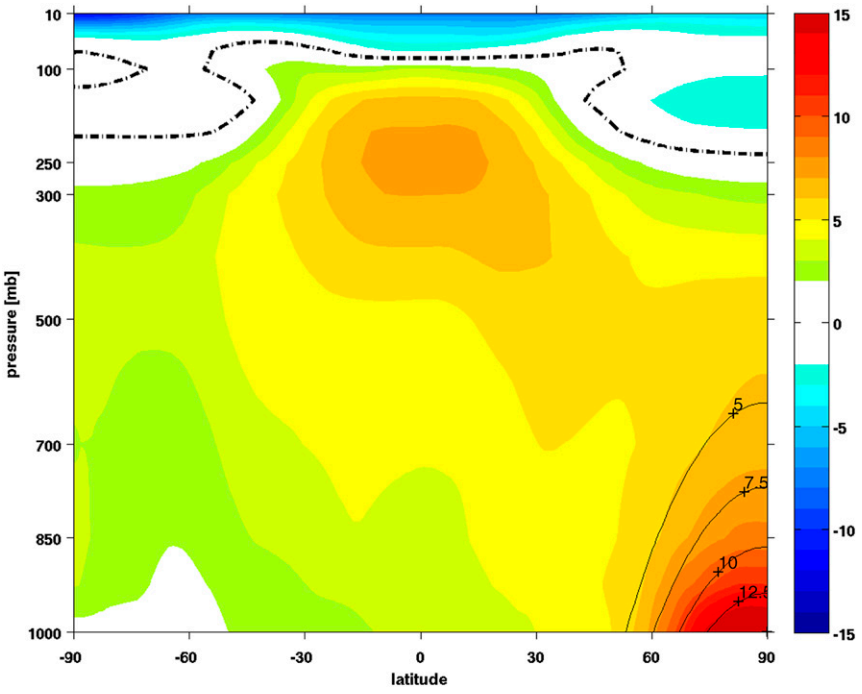

FIG. 1. Zonal-mean temperature response (K) in the RCP8.5 scenario averaged across 30 CMIP5 models (shown in color shadings; thick black dashed–dotted line denotes zero value). The anomaly is the average of November–December of 2080–99 relative to 1980–99 of historical runs. Thin black contours plot T_{eq}^{AA} as in Eq. (2) with $T_0^{AA} = 15$ K, $k = 5$, and $m = 3$.

divergence, and temperature in the stratosphere are nudged toward the reference state in the CTRL experiment. This is done via a simple relaxation in spectral space at every time step: $-K(\sigma)(X - X_0)/t_N$, where X is the instantaneous value of a given field (vorticity, divergence, or temperature), X_0 is the reference state, t_N is the nudging time scale (we choose a nudging time scale of 6 times the integration time step), and $K(\sigma)$ is the nudging coefficient that is 1 above 28 hPa, 0 below 64 hPa, and linear interpolation in between. The essence of the nudging method is that it shuts down the stratosphere–troposphere coupling by fixing the stratospheric zonal mean state at every time step. We construct the NUDG AA experiment where we impose AA-like forcing near the surface while nudging the stratospheric zonal mean state to that of the CTRL experiment. Then in the NUDG AA experiment, the response in the midlatitude troposphere is purely via the tropospheric pathway and is accomplished by tropospheric waves and wave–mean flow interaction. If we assume that the circulation response via the tropospheric and stratospheric pathways is linearly additive, then the stratospheric contribution to the total response can be obtained by the difference of the total response and response via the tropospheric pathway only in the nudging experiment. To confirm the stratospheric pathway, we also perform a NUDG downward-AA experiment by nudging the stratospheric zonal mean state to that of the AA experiment and imposing no thermal forcing near the surface.

Finally, we make use of a zonally symmetric version of the SFK10 model. Following Kushner and Polvani (2004), we first construct the eddy forcing, at each time step, as the negative tendency of the zonal and time mean state of the primitive equation model, and then use the computed eddy forcing to drive the zonally symmetric model. The zonally symmetric configuration has been widely used and is useful to further separate the direct thermally forced response and the effect of eddy feedbacks, specifically in the troposphere and in the stratosphere, respectively. As in Kushner and Polvani (2004), we perform a ZSYM E^{strat} experiment with the eddy forcing confined in the stratosphere by applying a smooth weighting function to the eddy forcing.

Table 1 lists a summary of all the experiments performed in this study.

c. *Diagnostics*

We estimate the magnitude of AA as the Arctic (67.5°–90°N) near-surface temperature increase in T_{eq}^{AA}. In the AA5, AA10, AA15, AA20, and AA25 experiments, the AA is about 3.49, 6.97, 10.46, 13.94, 17.43 K, respectively. As described above, the AA15 experiment

TABLE 1. Details of the model experiments. Here we show the AA15 experiment as an example; however, the details of all the experiments with other forcing magnitudes are the same.

Experiment name	Description
CTRL	Control experiment with SFK10 model.
AA15	AA experiment with imposed AA-like thermal forcing as in Eq. (1) with $T_0^{AA} = 15$ K.
NUDG AA15	Nudging experiment by nudging the stratospheric zonal mean state toward that of the CTRL while imposing AA-like thermal forcing.
NUDG downward-AA15	Nudging experiment by nudging the stratospheric zonal mean state toward that of the AA15 and imposing no AA-like forcing.
ZSYM E^{strat}	Zonally symmetric model experiment by applying the eddy forcing perturbation only in the stratosphere; the eddy forcing perturbation is computed in the AA15 experiment.

is close to the RCP8.5 scenario at the end of the twenty-first century. As in Table 12.2 of Collins et al. (2013), the projected annual mean Arctic temperature increase is about 8.3 ± 1.9 K across CMIP5 models, and our imposed AA forcing strength in AA15 is slightly larger because of the focus on winter season.

Second, to diagnose wave–mean flow interaction, we use the Eliassen–Palm (EP) flux in spherical and pressure coordinates, given by $\mathbf{F} = [F_{(\phi)}, F_{(p)}]$, and it is calculated as $F_{(\phi)} = -a\cos\phi\langle u^*v^*\rangle$ and $F_{(p)} = af\cos\phi(\langle v^*\theta^*\rangle/\langle\theta\rangle_p)$, where f is the Coriolis parameter, θ is potential temperature, u and v are the zonal and meridional wind velocities, angle brackets denote zonal average, and an asterisk denotes deviation from zonal average (Edmon et al. 1980). The direction of the flux vectors generally indicates the propagation of waves and the flux divergence, calculated as

$$\frac{1}{a\cos\phi}\nabla\cdot\mathbf{F} = \frac{1}{a\cos\phi}\left\{\frac{1}{a\cos\phi}\frac{\partial}{\partial\phi}[F_{(\phi)}\cos\phi] + \frac{\partial}{\partial p}F_{(p)}\right\},$$

measures the wave forcing on the zonal mean flow.

Third, we make use of two methods to identify SSW events, which are dramatic dynamical events in the NH and are characterized by a rapid increase of polar cap temperature and a reversal of westerly wind. The first is a standard method, which identifies a SSW when the daily zonal-mean zonal wind at 10 hPa, cosine weighted and averaged over 60°–90°N, drops below zero, with at least 45 days between two SSW events (e.g., Charlton and Polvani 2007; Butler et al. 2015). The second is the NAM method. The NAM at each pressure level is defined as the first EOF of daily zonal-mean zonal wind anomalies poleward of 20°N, weighted by the square root of the cosine of latitude, and then the NAM index is generated by projecting the unweighted original anomalies onto the first EOF, further standardized to unit variance. So the positive phase of the NAM, at 10 hPa for example, is associated with positive zonal wind poleward of about 45°N. A SSW event is defined to occur when the 10-hPa NAM index drops below −2.0 standard deviations and again with at least 45 days between two SSW events (e.g., Gerber and Polvani 2009, hereafter GP09). By using these two methods, we aim to provide a robust assessment of the SSW response to imposed AA.

Last, a couple of technical notes. Almost all the numerical experiments are integrated for 20 000 days with the first 1000 days of spinup discarded, and the zonally symmetric model experiments are run for 2000 days. For most climate variables, time averages are taken during the first 9000 days (averages over 9000 days are sufficient, and similar results are obtained with the last 10 000 days of integrations), except for SSW when 19 000 days are included. For all variables, statistical significance is evaluated via a simple Student's t test, using the 95% confidence interval. For the calculation of SSW frequency, the confidence interval is constructed by using the bootstrap method, which independently resamples the results with replacement for 1000 times. The confidence interval is then calculated as the 2.5th and 97.5th percentiles from resamplings.

3. Results

a. *Circulation response in troposphere and stratosphere*

First, Fig. 2a shows the climatological zonal-mean zonal wind in the SFK10 model. The simulated circulation mimics the NH perpetual winter conditions, which are characterized by a strong NH stratospheric polar vortex and a midlatitude jet located near 40°N in the lower troposphere.

As a result of imposed AA-like forcings, for various forcing strengths, the circulation response robustly exhibits an equatorward shift of the NH tropospheric jet, with a weakening of the zonal wind on the poleward flank and a strengthening on the equatorward flank. This is perhaps not surprising and is in agreement with many

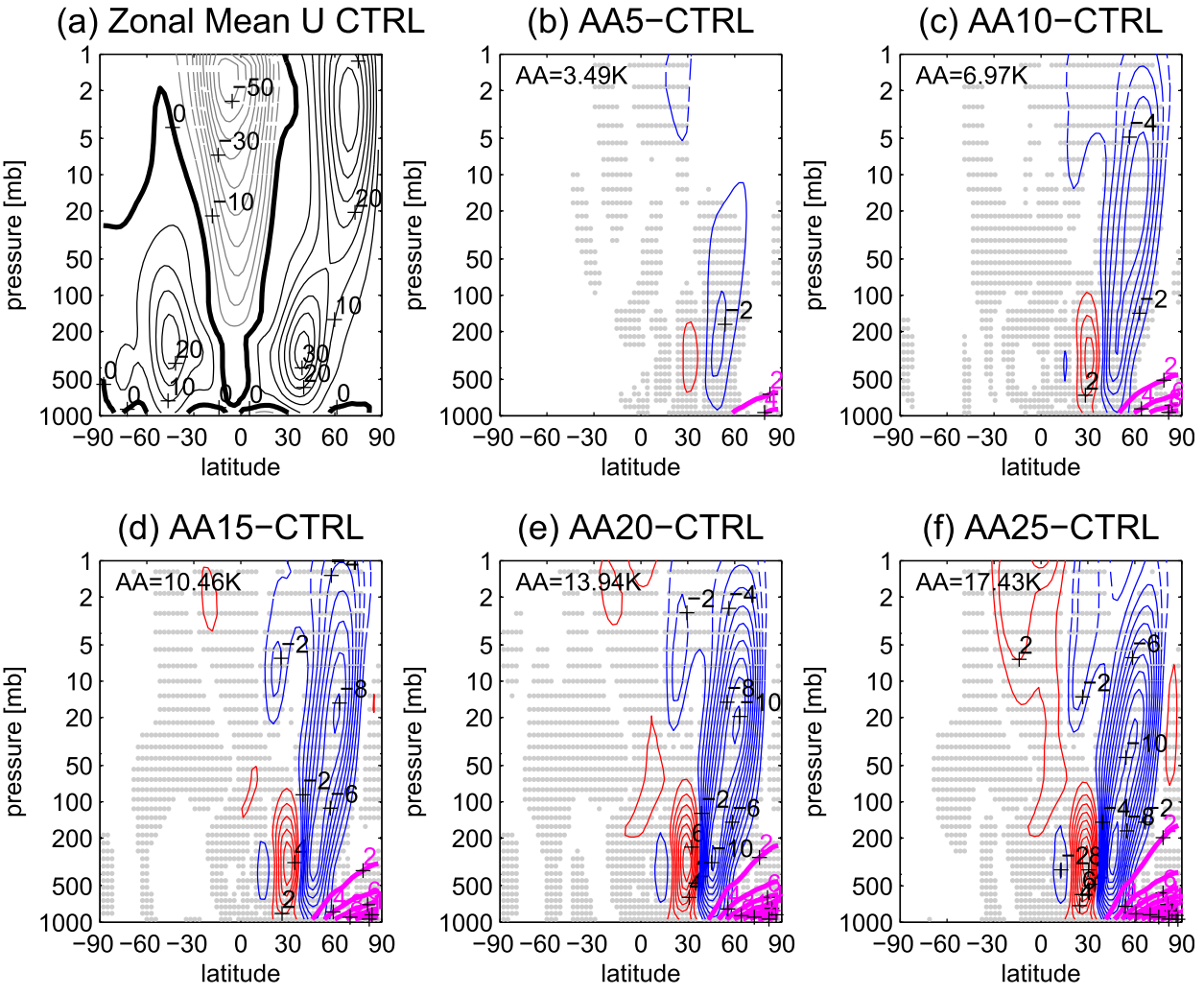

FIG. 2. (a) Zonal-mean zonal wind in CTRL (with the SFK10 model version); response of zonal-mean zonal wind in the (b) AA5, (c) AA10, (d) AA15, (e) AA20, and (f) AA25 experiments. The contour interval (CI) is 5 m s^{-1} in (a), with black contours for positive values, gray contours for negative values, and thick black contours for zero values. The CI is 1 m s^{-1} in (b)–(f), with red for positive and blue for negative. The magenta contours plot T_{eq}^{AA} as in Eq. (2) with CI = 2 K. The numbers in the top-left corner of (b)–(f) indicate the magnitude of AA, which is the near-surface temperature increase poleward of 67.5°N in T_{eq}^{AA}. Statistically significant responses, at the 95% level, are dotted.

previous studies (e.g., Deser et al. 2004; Peings and Magnusdottir 2014). More importantly, there is a robust weakening of the stratospheric polar vortex, which was also identified in some previous studies (e.g., Peings and Magnusdottir 2014; Feldstein and Lee 2014; Kim et al. 2014). The weakening of the stratospheric polar vortex appears to be coupled with the equatorward displaced tropospheric jet, which resembles the negative phase of NAM. In our model configuration, there appears to be no response in the Southern Hemisphere. When the AA-like forcing is weak, as in Fig. 2b, the tropospheric jet response is also rather weak and the stratospheric response is confined to the lower stratosphere. As the forcing becomes larger, the circulation response also becomes stronger (Fig. 2f).

To better quantify the zonal-mean zonal wind response, Fig. 3 shows the position and strength of maximal wind at 841, 256, and 10 hPa. The zonal-mean zonal wind is first interpolated onto a 0.1° grid using a cubic spline interpolation before calculating the jet latitude and intensity. In the lower troposphere, in response to AA-like forcings, the jet position moves equatorward and the maximal wind speed decelerates. In the upper troposphere, the jet also shifts equatorward but the maximal wind speeds up slightly. It is noted that the thermal wind balance approximately holds here, where the decrease in meridional temperature gradient is in balance with the decrease of zonal wind with altitude (not shown). In the stratosphere there is a general

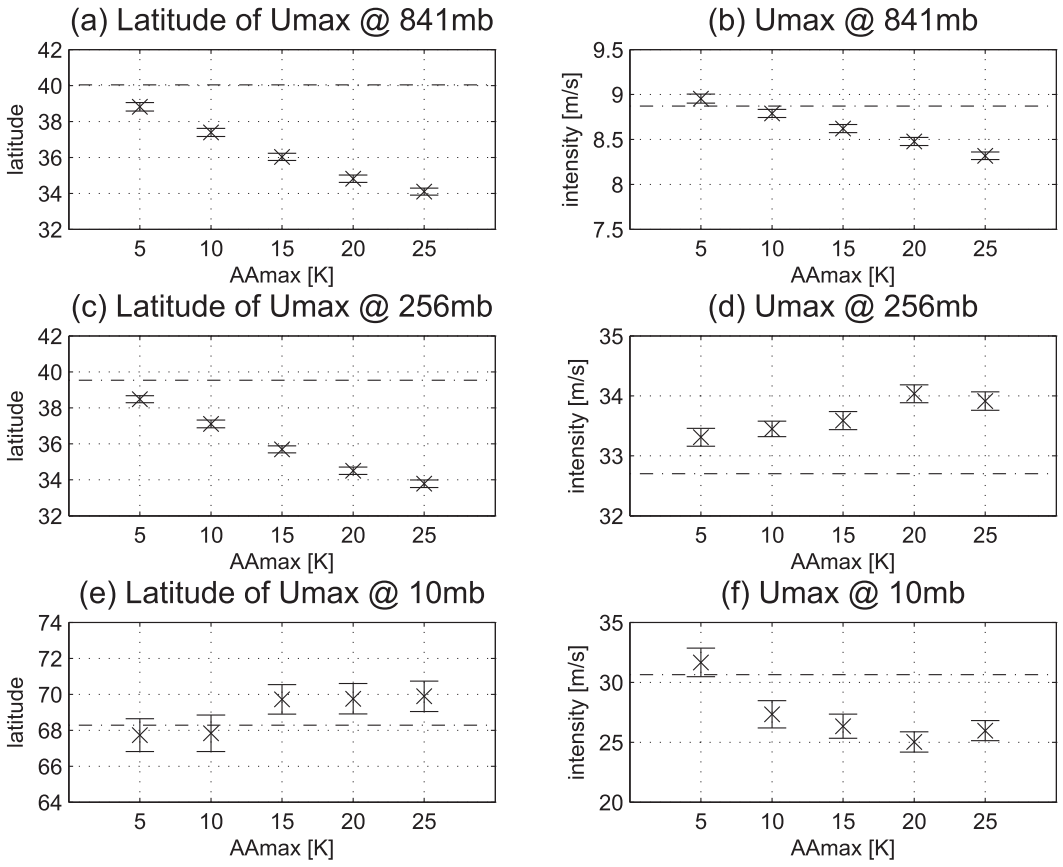

FIG. 3. (left) Latitude and (right) intensity of maximal zonal-mean zonal wind for CTRL and AA experiments at (a),(b) 841; (c),(d) 256; and (e),(f) 10 hPa. The results are plotted in dashed–dotted lines for CTRL and crosses for the AA experiments with error bars showing two standard deviations.

poleward displacement and weakening of the polar vortex. In the AA15 experiment, which is similar to the projected AA in the RCP8.5 scenario, the lower-tropospheric jet shifts equatorward by about 4° latitude and weakens by about 0.5 m s^{-1}, the upper-tropospheric jet shifts equatorward by 4° latitude and strengthens by 0.5 m s^{-1}, and the stratospheric jet moves poleward by 2° latitude and weakens by 5 m s^{-1}. Although in general, the larger the forcing, the larger the response, there also appears to be a tendency for the response to saturate.

To better interpret the weakening of the stratospheric polar vortex, Figs. 4a,b show the EP flux and its divergence in the control and AA15 experiment, as an example. The climatological flux vectors clearly indicate that the waves are generated in the lower troposphere, presumably as a result of baroclinic instability and orographic forcing, and propagate upward and equatorward. The response to imposed AA forcing shows more upward-propagating waves poleward of about 62°N as well as wave anomalies propagating northward in the stratosphere poleward of 62°N above 100 hPa. It is largely the northward flux anomaly and its convergence of momentum flux that contribute to an increase of net EP flux convergence (i.e., $\nabla \cdot \mathbf{F} < 0$) in the stratosphere and a weakening of the polar vortex. In the midlatitude troposphere, the response in EP flux is almost opposite in sign to that of the climatology and is associated with the equatorward tropospheric jet shift. This EP flux response is qualitatively similar in other forcing strength experiments (not shown).

Furthermore, to better understand the response in wave activity in our idealized experiments, we follow the method in SFK10 and decompose the response in eddy meridional heat flux into time-mean (TM) linear, time-mean nonlinear, and fluctuation (FL) components:

$$\Delta\overline{\langle v^* T^* \rangle} = \mathrm{TM}_{\mathrm{LIN}} + \mathrm{TM}_{\mathrm{NONLIN}} + \mathrm{FL},$$
$$\mathrm{TM}_{\mathrm{LIN}} = \langle (\Delta\overline{v}^*)\overline{T}^*_c \rangle + \langle (\Delta\overline{T}^*)\overline{v}^*_c \rangle,$$
$$\mathrm{TM}_{\mathrm{NONLIN}} = \langle \Delta\overline{T}^* \Delta\overline{v}^* \rangle, \quad \text{and}$$
$$\mathrm{FL} = \Delta\langle \overline{v^{*\prime} T^{*\prime}} \rangle,$$

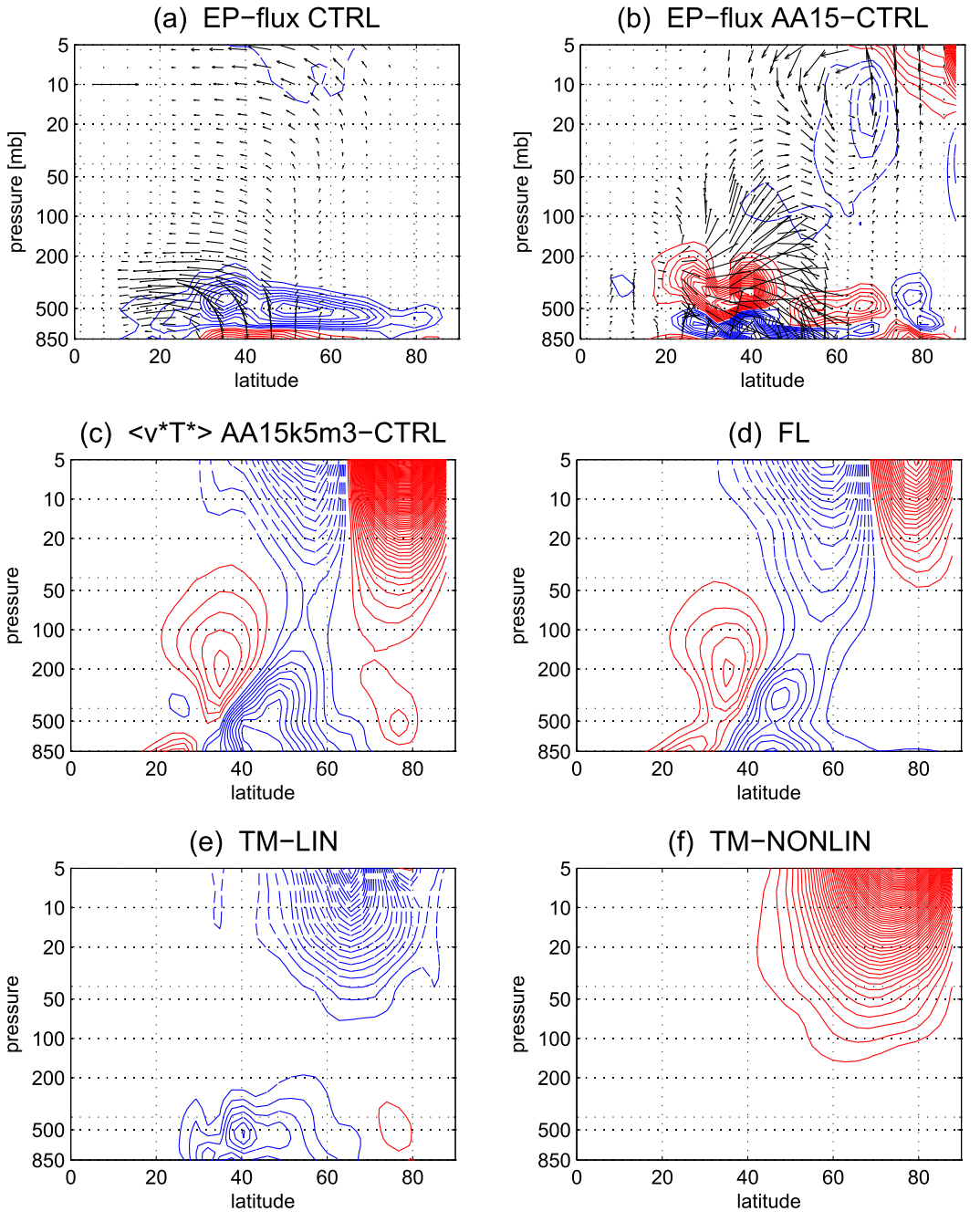

FIG. 4. (a) EP flux in CTRL and (b) its response to AA15. The EP flux vectors are scaled according to Eq. (3.13) of Edmon et al. (1980), and the horizontal arrow scale(10^{15} m^3) is indicated in the top-left corner of (a). The EP flux vectors in (b) are scaled by a factor of 20. The CI is 1 m s^{-1} day^{-1} in (a) and 0.2 m s^{-1} day^{-1} in (b) with red contours for positive values and blue for negative. (c) Response in eddy meridional heat flux and its decomposition into the (d) high-frequency wave FL term, (e) time-mean linear term (TM_{LIN}), and (f) time-mean nonlinear term (TM_{NONLIN}). The CI is 0.5 K m s^{-1} in (c)–(f).

where v and T are daily variables, Δ is the difference between AA and control experiment, subscript c denotes the control experiment, bar denotes time average, prime denotes deviation from time average, angle brackets denote zonal average, and an asterisk denotes deviation from zonal average. In the prescribed Siberian snow forcing experiments of SFK10 with the same model setup, linear interference was found to work well to explain the response in wave activity, which was dominated by the TM_{LIN} component, and wave activity

was amplified in constructive interference when the wave anomaly was in phase with the climatology. The FL term, which is associated with high-frequency wave components, and TM_{NONLIN} were found to be small.

However, the heat flux decomposition seems more complicated in our imposed AA forcing experiments, and linear interference is not the dominant mechanism at high latitudes. Figures 4c–f show the response in zonal-mean eddy heat flux and its decomposition. The response in meridional heat flux shows an increase at high latitudes and a decrease in midlatitudes, which is in agreement with the response in EP flux (Fig. 4b). Although our AA forcing is zonally symmetric, the interaction between the AA forcing and the zonally asymmetric lower boundary condition excites planetary-scale Rossby waves at high latitudes (primarily wave 1, not shown). The increased heat flux at high latitudes is mostly due to the nonlinear component and, to a lesser extent, the high-frequency wave contribution. The linear component seems to contribute to the increased heat flux in the troposphere high latitudes but certainly not in the stratosphere high latitudes.

This seems to be different from some previous studies that found increased upward wave propagation as a result of the sea ice loss over the B-K Seas and attributed the mechanism to wave constructive interference (e.g., Peings and Magnusdottir 2014; Feldstein and Lee 2014; Kim et al. 2014; Sun et al. 2015). Although we do not have a full explanation yet, the model setup and imposed forcing are completely different in our study. The model is a dry primitive equation model and may have some deficiencies in fully capturing the circulation at high latitudes. More importantly, we impose a zonally symmetric forcing whereas previous studies all focused on regional sea ice loss and associated surface flux and temperature increase. A study by Garfinkel et al. (2010) examined the tropospheric precursors to stratospheric polar vortex weakening and found the North Pacific low and the eastern European high most effective in modulating the polar vortex. A low anomaly of geopotential height—for example, during the October snow anomaly over Eurasia—could constructively interfere with the climatological northwestern Pacific low and amplify the wave activity into the stratosphere, resulting in a weakening of the polar vortex, as seen in Cohen et al. (2007) and SFK10. The sea ice loss over the B-K Seas along with the resulting high geopotential height anomaly happens to be collocated with the eastern European high and could effectively increase the upward wave propagation into the stratosphere (e.g., Kim et al. 2014). However, this is not the same in our study. A zonally symmetric forcing over the entire Arctic could excite more complicated waves and the mechanism of linear interference might no longer play a dominant role.

Figure 5 shows the zonal wind response at 513 hPa. In the control experiment, the zonal wind peaks over the North American–North Atlantic sector and the Asian–North Pacific sector. The equatorward displacement of zonal wind, as a result of AA, is found to maximize over the North Atlantic and North Pacific sectors, which projects onto the climatological zonal wind pattern. The zonal wind response is generally robust across various forcing strengths.

Finally, since the time-mean stratospheric polar vortex weakens as a result of AA, next we assess whether there is a change in stratospheric variability—in particular, SSW frequency (e.g., Jaiser et al. 2013). First of all, in the control experiment, the SSW frequency is about 0.27 per 100 days as defined by the standard method with a reversal of zonal mean westerly wind at 10 hPa poleward of 60°N (Fig. 6a). A similar result is found using the NAM method (0.25 per 100 days, Fig. 6b). The SFK10 model underestimates the observed SSW frequency [e.g., Butler et al. (2015) estimated 0.91 per winter season from November to March, or equivalently about 0.61 per 100 days, using ERA-40 and ERA-Interim and similar reversal of westerly wind method]; however, this behavior is found to be rather common even among state-of-the-art climate models (e.g., Charlton-Perez et al. 2013). Figure 6 shows the SSW response and its confidence interval as a consequence of the imposed AA forcing. In general, both the standard and NAM methods[1] show no statistically significant change in the SSW frequency. The SSW response using the standard method is rather minor, except for the AA5 experiment, where a decrease compared to control is seen at marginal significance level. The response in the NAM method seems to show a small rising trend as AA strength increases, but this is not statistically significant, perhaps except for a marginally significant increase in the largest AA forcing experiment. We note here that the precise choice of the parameters in SSW definitions (such as the latitude and recovery period) has no effect on the conclusions drawn in this paper.

To aid the interpretation of the modeled SSW response to AA, Fig. 7 shows the time-mean meridional eddy heat flux $\langle v^* T^* \rangle$ at 100 hPa. It can be seen in Fig. 7a that, at middle-to-high latitudes, poleward of 45°N, the response in meridional heat flux exhibits a dipole

[1] For the calculation of the NAM index in various AA forcing strength experiments, we have also tried projecting the anomalies onto the first EOF from the CTRL experiment and have obtained nearly identical results.

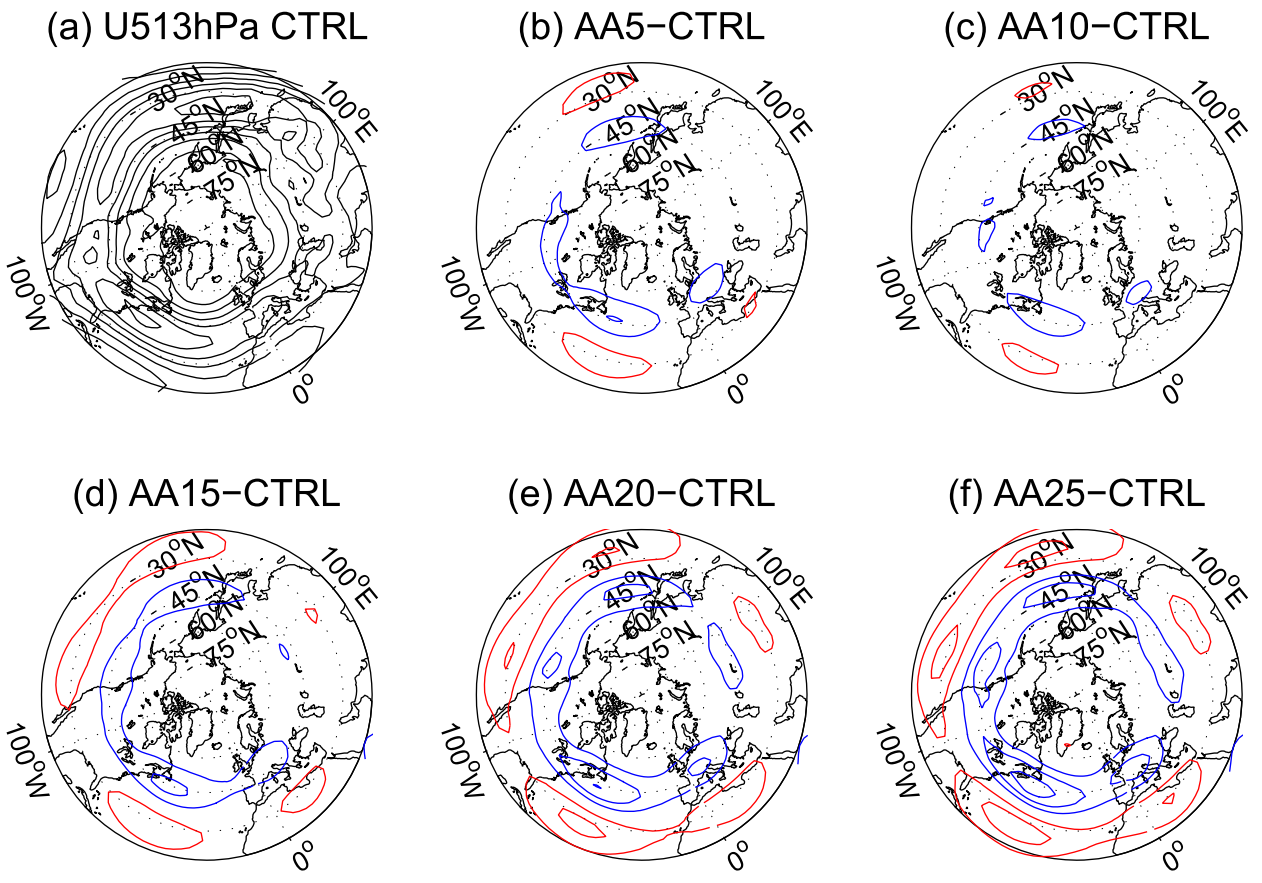

FIG. 5. As in Fig. 2, but for zonal wind over NH at 513 hPa. The CI is 5 m s^{-1} in (a), 2 m s^{-1} in (b), and 5 m s^{-1} in (c)–(f).

structure, with an increase northward of 60°N and a decrease equatorward. The increase of meridional heat flux at high latitudes is likely due to the near-surface AA and resulting increased upward planetary-scale wave propagation. The equatorward shift of the tropospheric jet is associated with an equatorward shift of the baroclinic instability zone and therefore the meridional heat flux, leading to a decrease of $\langle v^*T^* \rangle$ over 45°–60°N. Figure 7b shows the average of $\langle v^*T^* \rangle$ poleward of 45°N, weighted by the cosine of latitude, and the change is rather small compared to the control experiment (i.e., only about 2% for most of the forcing strengths). This is due to the cancellation between the increase at high latitudes and decrease at midlatitudes. Therefore, in summary, we find that there is no significant change in net meridional heat flux at middle-to-high latitudes, and this seems to be in agreement with no significant change in SSW frequency as a result of AA.

b. *The role of troposphere and stratosphere pathway*

The equilibrium circulation response, as seen in Fig. 2, likely consists of the response via both tropospheric and stratospheric pathway. The tropospheric circulation response via the tropospheric pathway is associated with the adjustment of transient eddies, because of the change in meridional temperature gradient and baroclinic instability. On the other hand, the stratospheric pathway involves enhanced upward planetary-scale wave propagation and the weakening of the stratospheric polar vortex as a result of AA that could modify the tropospheric circulation response. To distinguish the two pathways, we "deactivate" the stratospheric pathway by nudging the stratospheric zonal mean state toward a reference state in the CTRL experiment (details described in section 2). As described above, although waves can propagate freely into the stratosphere, they have almost no influence on the stratospheric zonal mean state because of the nudging, and therefore, there is no zonal mean anomaly that could propagate downward back to the troposphere.

Before discussing the key results, we first demonstrate that the nudging method is indeed acting to largely damp the zonal mean stratospheric variability. Figure 8 shows the amplitude of the NAM pattern of variability in the CTRL and NUDG experiments. Following Gerber et al. (2010) and Simpson et al. (2013), we first

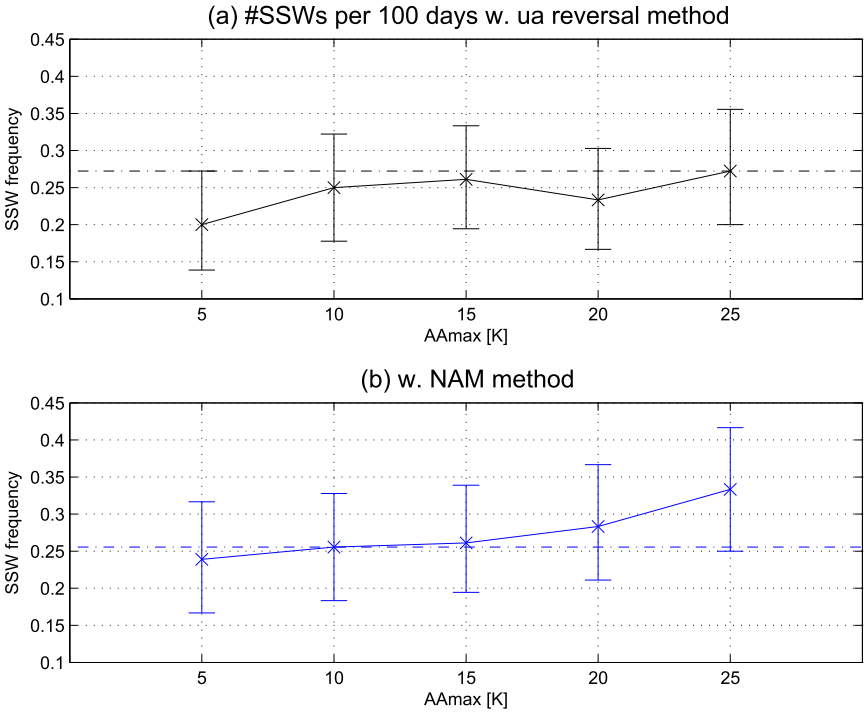

FIG. 6. SSW frequency in CTRL and AA experiments using (a) the standard method with reversal of westerly wind and (b) the NAM method. The results are plotted in dashed–dotted lines for CTRL and crosses for the AA experiments with error bars showing the 2.5th and 97.5th percentiles using the bootstrapping method.

compute the NAM and NAM index (as above in the calculation of SSW). We then construct the NAM pattern by regressing the daily zonal-mean zonal wind anomalies onto the NAM index and compute the NAM amplitude as the root-mean-square of the NAM pattern weighted by the cosine of latitude. In Fig. 8, the CTRL experiment shows a tropospheric NAM pattern of variability, maximized in the middle-to-upper troposphere, and a larger stratospheric variability that increases with height. We also show the same diagnostic for the nudging experiments, and it is clear that, in all the nudging experiments, the stratospheric variability is largely reduced while the tropospheric variability is essentially unaffected.

Next we choose AA15 as a primary example to demonstrate the tropospheric and stratospheric pathway, and other forcing strengths are qualitatively similar. Figures 9a–c show the zonal-mean zonal wind in the CTRL and AA15 experiment and their difference, respectively, which is similar to Fig. 2d. Figure 9d shows the zonal-mean zonal wind in the nudging experiment and Fig. 9e shows the response, which is obtained via the tropospheric pathway only. As shown in Fig. 9e, the stratospheric zonal mean state is largely unaffected and the tropospheric circulation exhibits an equatorward displacement with a decrease in zonal wind on the poleward flank and an increase on the equatorward flank, which is similar in pattern but smaller in magnitude than the total response seen in Fig. 9c. Results are found to robust with the last 10 000 days of integrations (not shown). We also note here that we perform an additional NUDG CTRL experiment, in which we nudge the stratospheric zonal mean state toward that of the CTRL. We find that the zonal-mean zonal wind in both the troposphere and stratosphere in the NUDG CTRL experiment is almost identical to that of the CTRL experiment (not shown).

If we assume that the circulation responses via the tropospheric pathway and stratospheric pathway are linearly additive, the difference between the total response and the response via the tropospheric pathway can be interpreted as the response via the stratospheric pathway and stratosphere–troposphere coupling (Fig. 9f). The response via the stratospheric pathway shows a weakening of the stratospheric polar vortex as well as an equatorward shift of the tropospheric jet, which resembles the downward influence from the stratosphere on the troposphere as found in many previous studies such as Baldwin and Dunkerton (2001). This effect on the tropospheric circulation is certainly

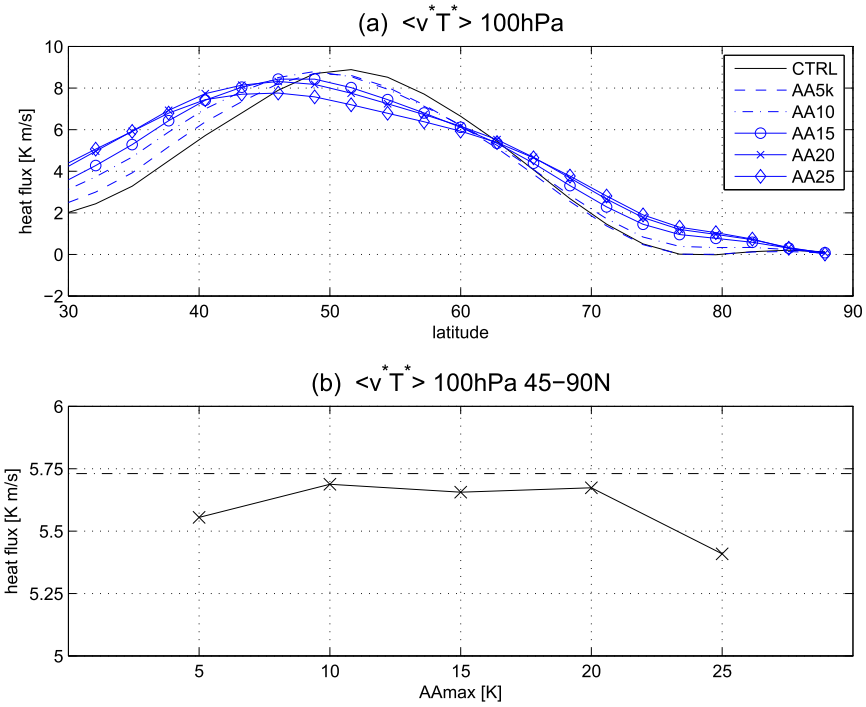

FIG. 7. Eddy meridional heat flux (a) at 100 hPa and (b) averaged poleward of 45°N in CTRL and AA experiments.

nonnegligible and is, in fact, similar in magnitude to that via the tropospheric pathway only. This suggests that the stratospheric pathway and stratosphere–troposphere coupling play a significant role in determining the midlatitude tropospheric circulation response to AA.

Next we confirm that the circulation response, as seen in Fig. 9f, is indeed the downward influence from the stratosphere on the troposphere. To do that, we nudge the stratospheric zonal mean state to that of the AA15 experiment (as in Fig. 9b) with no prescribed thermal forcing near the surface. Figure 10a shows the circulation response in this NUDG downward-AA15 experiment. The response is almost identical to Fig. 9f. In particular, the equatorward shift of the tropospheric jet is indistinguishable from that of Fig. 9f, confirming that this is indeed the downward influence of the stratosphere on the troposphere. In addition, we note here that the circulation response via the stratospheric pathway is accomplished not only by stratospheric wave–mean flow interaction but also by the tropospheric eddy feedback. To briefly demonstrate this, we examine the circulation response in the zonally symmetric model configuration. First, we confirm that when the eddy forcing is applied, the zonally symmetric model is able to reproduce the total response in the full model as seen in Fig. 9c (the zonally symmetric model result is not shown). Then, we investigate the importance of downward control to the tropospheric response by confining the eddy forcing to the stratosphere only (Haynes et al. 1991; Kushner and Polvani 2004). By eliminating the tropospheric eddy feedback, Fig. 10b shows that, although the stratospheric wind response is able to penetrate into the troposphere, there is no clear equatorward shift of the jet and no coupling to the surface. This is in agreement with previous studies such as Kushner and Polvani (2004) and Domeisen et al. (2013). Thus, we conclude that the circulation response is indeed the downward influence from the stratosphere on the troposphere and requires tropospheric eddy feedback in addition to stratospheric eddy forcing.

Finally, in order to quantitatively measure the role of an active stratosphere, we calculate the jet position and intensity as in Fig. 3 but now including the results of the NUDG AA experiments (Fig. 11). Again the jet position and intensity in the stratosphere in the nudging experiments, by design, is largely unaffected (Figs. 11e,f). However, in both the lower and upper troposphere, consistently for various forcing strengths, the response via the tropospheric pathway is almost always about half of the total response and the other half is accomplished via the stratospheric pathway. Therefore, in summary, by using the nudging method, we are able to explicitly separate the tropospheric and stratospheric pathway. We find that, in response to AA, coupling between the stratosphere and the troposphere significantly enhances

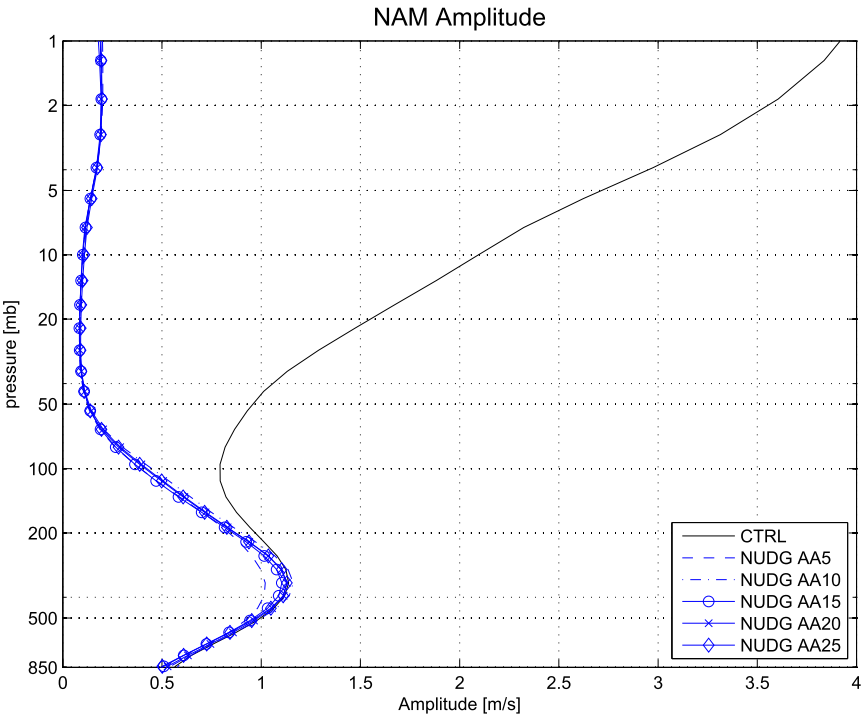

FIG. 8. NAM amplitude as a function of pressure levels in CTRL and NUDG AA experiments. See text for details in the calculation of NAM amplitude.

the midlatitude tropospheric circulation response by shifting the tropospheric jet farther equatorward.

A final note before concluding—the effect of the stratospheric pathway is found to be robust in a slightly different model configuration. In addition to SFK10, we also perform a similar set of AA and NUDG AA experiments using the GP09 configuration with an idealized wave-2 topography. With the GP09 model version and some modifications to simulate a tropospheric jet with a more realistic location (near 42°N), we find qualitatively similar results and the stratospheric pathway also significantly shifts the tropospheric jet equatorward. Details of the model setup and results are provided in the appendix and Fig. 12, respectively.

4. Discussion and conclusions

We have examined the NH midlatitude circulation response to imposed AA-like thermal forcing in a simple AGCM. In particular, we have focused on two key aspects—first, on the robust circulation response in the troposphere and stratosphere and second, on the role of stratosphere–troposphere coupling in determining the midlatitude circulation. For the first part, we have found that, as a result of AA, the tropospheric jet shifts equatorward and the stratospheric polar vortex weakens, which is robust for various forcing strengths. We have also calculated the frequency of SSWs and found no statistically significant change in SSWs, which is in agreement with no significant change in meridional heat flux.

For the second part, we have explicitly separated the tropospheric and stratospheric pathway by nudging the stratospheric zonal mean state in the AA experiments to the reference state in the control. We have found that, by shutting down the stratosphere–troposphere coupling, the tropospheric circulation still shifts equatorward but to a lesser extent (about half the magnitude). As for the tropospheric pathway and its underlying mechanism, it was discussed extensively in Deser et al. (2004) and others and is beyond the scope of this study. The difference between the total and nudged response, which we argue represents the stratospheric pathway (i.e., the downward influence of the stratosphere on the troposphere), also shows an equatorward shift of the tropospheric jet, similar in magnitude to that of the tropospheric pathway. Therefore, this suggests that an active stratosphere along with its coupling with the troposphere plays a significant role in determining the tropospheric circulation response to AA.

In this study, we have demonstrated, for the first time, that the stratospheric pathway could be potentially as important as the tropospheric pathway. Although Sun et al. (2015) found a stronger circulation response to Arctic sea ice loss in high-top WACCM4 compared to

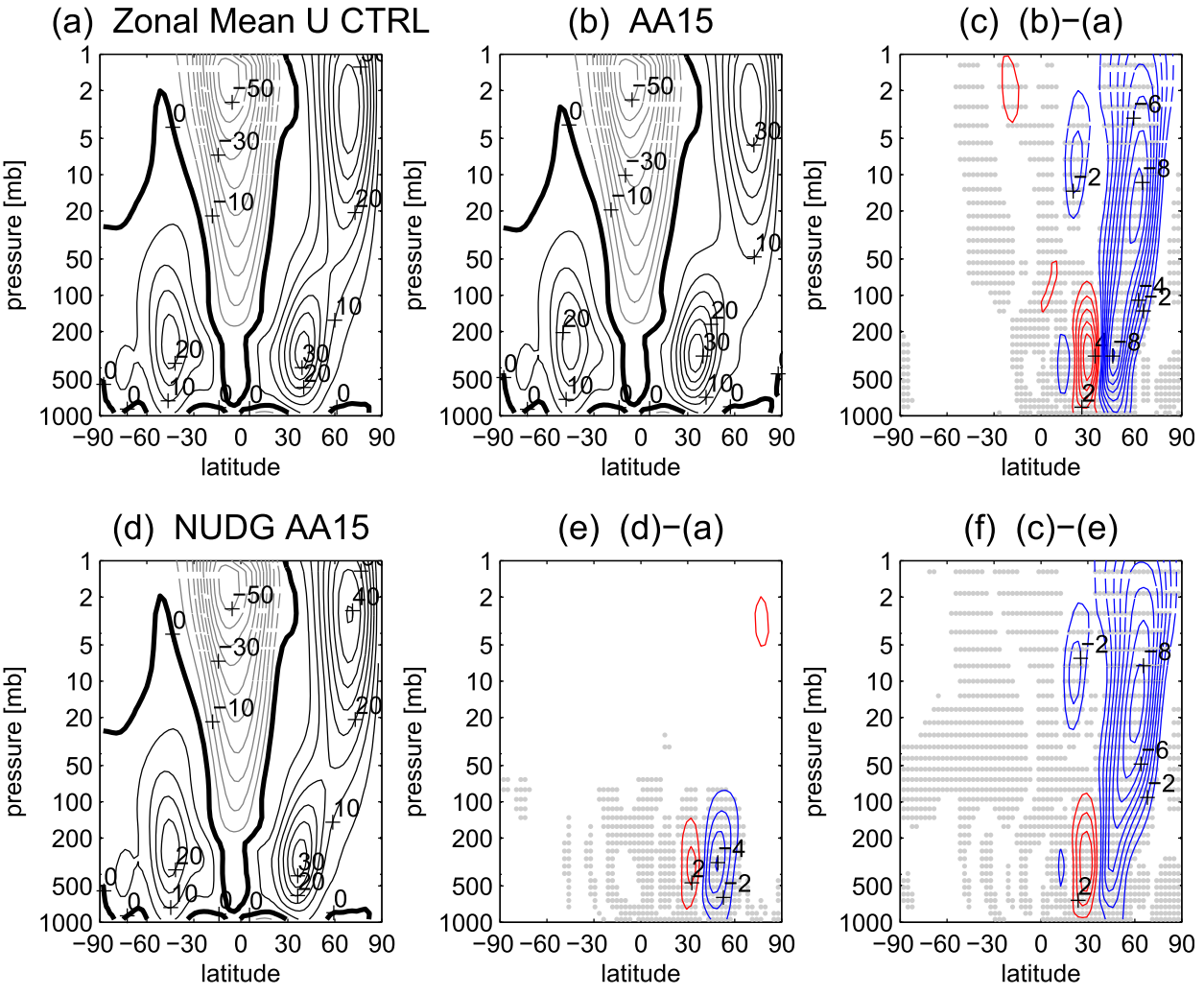

FIG. 9. Zonal-mean zonal wind in (a) CTRL and (b) AA15 experiments and (c) their difference. (d) Zonal-mean zonal wind in the NUDG AA15 experiment and (e) its change compared to CTRL (can be considered as the response via the troposphere only). (f) The difference in zonal wind response between (c) and (e) (which can be considered as the response via the stratospheric pathway only). Note that (a) and (c) are similar to Figs. 2a and 2d, respectively. The CI is 5 m s^{-1} in (a),(b),(d) and 1 m s^{-1} in (c),(e),(f).

low-top CAM4 and suggested a stratospheric pathway, the two models have different climatological mean states and stratospheric variability and the underlying mechanisms are potentially complex. Here, we have presented a clearer separation of the tropospheric and stratospheric pathways using a single model, and we are able to quantitatively estimate the relative importance of the two pathways.

One possible caveat of this study is the use of zonally symmetric AA forcing. In future climate projections, the Arctic sea ice loss and AA are not zonally symmetric [e.g., Figs. 12.11 and 12.29 of Collins et al. (2013)]. In fact, as demonstrated in Sun et al. (2015), at the end of the century, most of the sea ice loss within the Arctic Circle is projected to occur in the B-K Seas and the Pacific outside the Arctic Circle. The effects from sea ice loss in these two sectors, however, tend to drive opposite responses in upward wave propagation and the stratospheric polar vortex. In future study, we plan to consider zonally asymmetric forcings in different regions. Second, this study is focused solely on the effect of AA in an idealized dry model, and the implication for future climate change needs to take many other factors into account such as the extensive warming in the tropical upper troposphere. Barnes and Polvani (2015) examined the projected changes in North American–North Atlantic circulation in CMIP5 models and found that AA might modulate some aspects of the circulation response but is unlikely to dominate. Finally, our study investigates the equilibrium

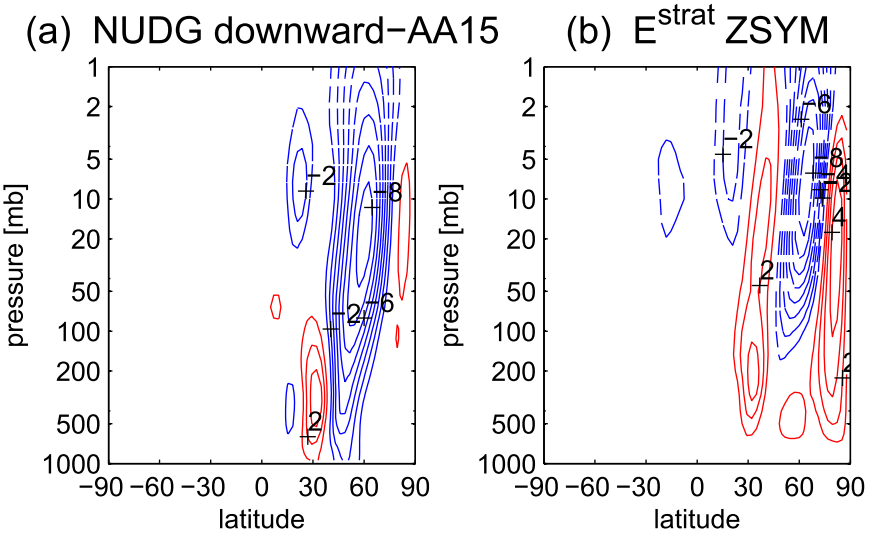

FIG. 10. Zonal-mean zonal wind response (a) in NUDG downward-AA15 experiment and (b) in ZSYM E^{strat}. The CI is 1 m s^{-1}.

circulation response in perpetual winter conditions and does not consider the possible delaying effect from the stratosphere. Sun et al. (2015) imposed sea ice loss only in autumn and found a significant tropospheric circulation response in late winter and early spring, possibly through the stratospheric pathway. We plan to further investigate the role of the stratospheric pathway in transient simulations in the future.

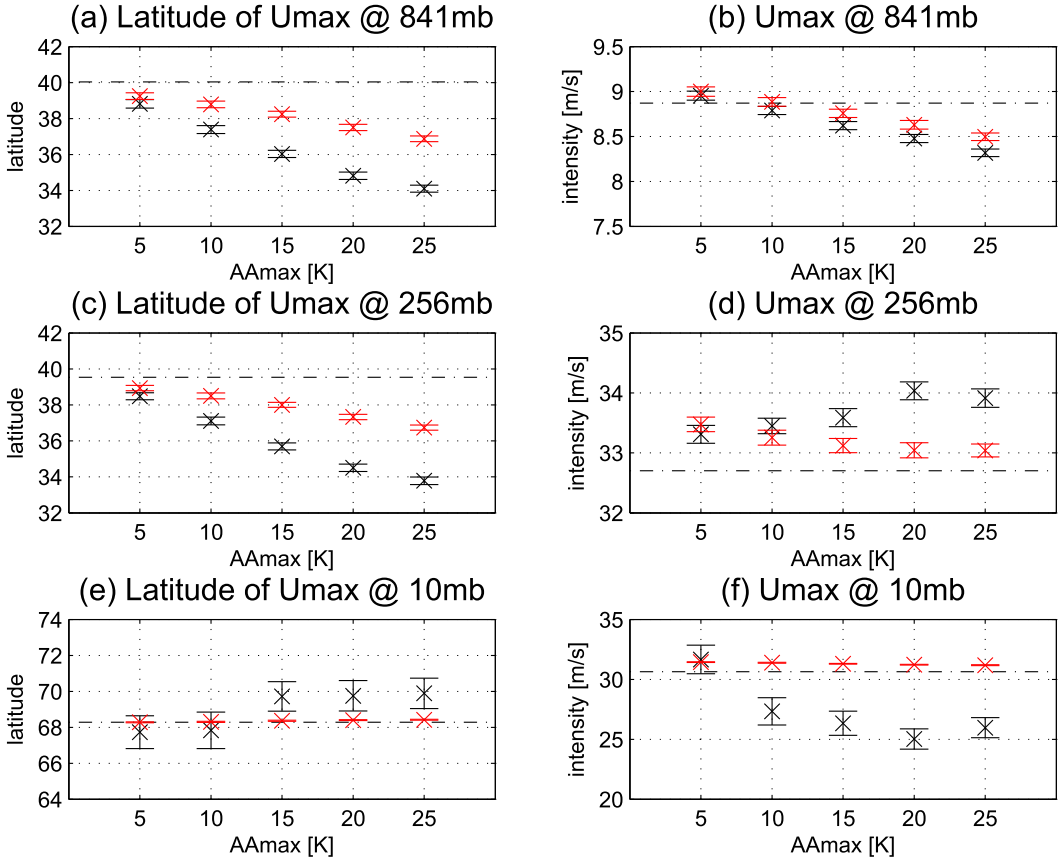

FIG. 11. As in Fig. 3, but including the results from NUDG experiments, plotted with red crosses and error bars.

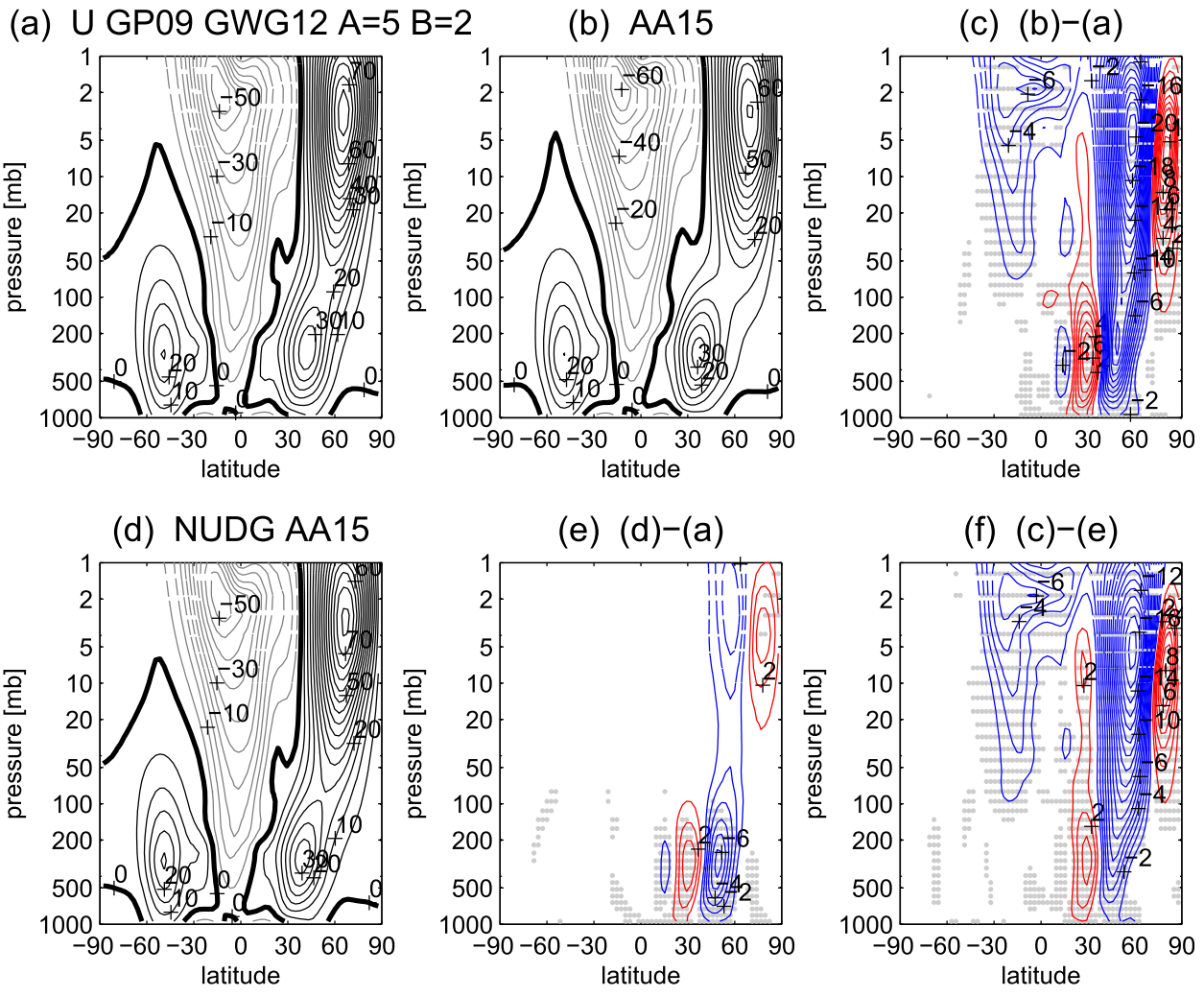

FIG. 12. As in Fig. 9, but using the GP09 model version with a tropospheric jet located near 42°N.

In this study, we have demonstrated that stratosphere–troposphere coupling plays a nonnegligible role in setting up the tropospheric circulation response to high-latitude near-surface warming. Our results provide further evidence that use of stratosphere-resolving GCMs is critical in order to fully simulate the circulation response to climate change (e.g., Charlton-Perez et al. 2013).

Acknowledgments. The authors thank Lorenzo M. Polvani and Clara Deser for helpful discussions. The authors acknowledge the World Climate Research Programme's Working Group on Coupled Modelling, which is responsible for CMIP, and we thank the climate modeling groups for producing and making available their model output. For CMIP the U.S. Department of Energy's Program for Climate Model Diagnosis and Intercomparison provides coordinating support and led development of software infrastructure in partnership with the Global Organization for Earth System Science Portals. YW is supported, in part, by the U.S. National Science Foundation (NSF) Climate and Large-Scale Dynamics program under Grant AGS-1406962. KLS is funded by a Natural Sciences and Engineering Research Council of Canada (NSERC) postdoctoral fellowship.

APPENDIX

Results in a Different Model Version

As described in section 2, we choose the SFK10 model because of the representation of the stratospheric circulation and its variability as well as the tropospheric jet position. Here we demonstrate the robustness of the results by using a slightly different model configuration that has also been widely used in the community.

We use the GP09 model version, in which $\gamma = 4\,\mathrm{K\,km^{-1}}$ and an idealized wave-2 topography is imposed. As demonstrated in GP09, the combination of $\gamma = 4\,\mathrm{K\,km^{-1}}$ and wave-2 topography has the most realistic stratosphere–troposphere coupling. While the GP09 model generates planetary-scale stationary waves and produces rather realistic stratospheric variability, the low-level jet is located near 30°N, which is a bit too equatorward compared to the observed wintertime jet position. To move the tropospheric jet northward to mimic the observed winter conditions, we follow Garfinkel et al. (2013) and add two additional terms to the T_{eq} equation, as in Eq. (2) of Garfinkel et al. (2013). By setting $A = 5$ and $B = 2$, we are able to shift the tropospheric jet to about 42°N. Figure 12a shows the zonal-mean zonal wind, and it has a tropospheric jet located at 42°N and a stronger stratospheric polar vortex than the SFK10 version.

However, we find that the frequency of SSWs is reduced by a large amount as the tropospheric jet moves poleward. With a jet near 30°N, the SSW frequency is about 0.3 per 100 days; however, with a jet near 42°N, the SSW frequency decreases to 0.08 per 100 days. This issue of SSW shutdown has also been identified in Wang et al. (2012) and is probably due to the regime behavior in model setup (E. Gerber 2015, personal communication). This issue could be a major concern in the discussion of stratosphere–troposphere coupling as SSWs are important dynamical events that have the potential to migrate downward and affect near-surface weather pattern (e.g., Baldwin and Dunkerton 2001; Polvani and Waugh 2004).

Nonetheless, we examine the midlatitude circulation response to imposed AA forcings in this model version, in particular, the role of stratosphere–troposphere coupling. In response to AA15, as an example, the stratospheric polar vortex shows a general weakening (with some strengthening at high latitudes), and the tropospheric jet moves equatorward (Fig. 12c). With the same nudging method applied in the stratosphere as NUDG AA, Fig. 12e shows the circulation response via the tropospheric pathway and has the tropospheric jet shifted equatorward as well, but to a lesser extent. Figure 12f shows the response via stratosphere–troposphere coupling, and it resembles the downward influence from the stratosphere on the troposphere. The zonal-mean zonal wind response is similar in the midlatitude troposphere between the tropospheric pathway (Fig. 12e) and stratospheric pathway (Fig. 12f). This demonstrates that an active stratosphere indeed acts to significantly intensify the tropospheric circulation response to AA, and this is in agreement with the SFK10 model configuration.

REFERENCES

Baldwin, M. P., and T. J. Dunkerton, 2001: Stratospheric harbingers of anomalous weather regimes. *Science*, **294**, 581–584, doi:10.1126/science.1063315.

Barnes, E. A., and L. Polvani, 2015: CMIP5 projections of Arctic amplification, of the North American/North Atlantic circulation, and of their relationship. *J. Climate*, **28**, 5254–5271, doi:10.1175/JCLI-D-14-00589.1.

——, and J. Screen, 2015: The impact of Arctic warming on the midlatitude jet-stream: Can it? Has it? Will it? *Wiley Interdiscip. Rev.: Climate Change*, **6**, 277–286, doi:10.1002/wcc.337.

Butler, A. H., D. W. J. Thompson, and R. Heikes, 2010: The steady-state atmospheric circulation response to climate change–like thermal forcings in a simple general circulation model. *J. Climate*, **23**, 3474–3496, doi:10.1175/2010JCLI3228.1.

——, D. Seidel, S. Hardiman, N. Butchart, T. Birner, and A. Match, 2015: Defining sudden stratospheric warmings. *Bull. Amer. Meteor. Soc.*, **96**, 1913–1928, doi:10.1175/BAMS-D-13-00173.1.

Cai, D., M. Dameris, H. Garny, and T. Runde, 2012: Implications of all season Arctic sea-ice anomalies on the stratosphere. *Atmos. Chem. Phys.*, **12**, 11 819–11 831, doi:10.5194/acp-12-11819-2012.

Charlton, A. J., and L. M. Polvani, 2007: A new look at stratospheric sudden warmings. Part I: Climatology and modeling benchmarks. *J. Climate*, **20**, 449–469, doi:10.1175/JCLI3996.1.

Charlton-Perez, A. J., and Coauthors, 2013: On the lack of stratospheric dynamical variability in low-top versions of the CMIP5 models. *J. Geophys. Res. Atmos.*, **118**, 2494–2505, doi:10.1002/jgrd.50125.

Cohen, J., and Coauthors, 2014: Recent Arctic amplification and extreme mid-latitude weather. *Nat. Geosci.*, **7**, 627–637, doi:10.1038/ngeo2234.

——, M. Barlow, P. J. Kushner, and K. Saito, 2007: Stratosphere–troposphere coupling and links with Eurasian land surface variability. *J. Climate*, **20**, 5335–5343, doi:10.1175/2007JCLI1725.1.

——, J. Foster, M. Barlow, K. Saito, and J. Jones, 2010: Winter 2009–2010: A case study of an extreme Arctic Oscillation event. *Geophys. Res. Lett.*, **37**, L17707, doi:10.1029/2010GL044256.

Collins, M., and Coauthors, 2013: Long-term climate change: Projections, commitments and irreversibility. *Climate Change 2013: The Physical Science Basis*, T. F. Stocker et al., Eds., Cambridge University Press, 1029–1136. [Available online at http://www.climatechange2013.org/images/report/WG1AR5_Chapter12_FINAL.pdf.]

Deser, C., G. Magnusdottir, R. Saravanan, and A. Phillips, 2004: The effects of North Atlantic SST and sea ice anomalies on the winter circulation in CCM3. Part II: Direct and indirect components of the response. *J. Climate*, **17**, 877–889, doi:10.1175/1520-0442(2004)017<0877:TEONAS>2.0.CO;2.

Domeisen, D. I. V., L. Sun, and G. Chen, 2013: The role of synoptic eddies in the tropospheric response to stratospheric variability. *Geophys. Res. Lett.*, **40**, 4933–4937, doi:10.1002/grl.50943.

Edmon, H. J., B. J. Hoskins, and M. E. McIntyre, 1980: Eliassen-Palm cross sections for the troposphere. *J. Atmos. Sci.*, **37**, 2600–2616, doi:10.1175/1520-0469(1980)037<2600:EPCSFT>2.0.CO;2.

Feldstein, S., and S. Lee, 2014: Intraseasonal and interdecadal jet shifts in the Northern Hemisphere: The role of warm pool tropical convection and sea ice. *J. Climate*, **27**, 6497–6518, doi:10.1175/JCLI-D-14-00057.1.

Fletcher, C. G., S. C. Hardiman, P. J. Kushner, and J. Cohen, 2009: The dynamical response to snow cover perturbations in a large ensemble of atmospheric GCM integrations. *J. Climate*, **22**, 1208–1222, doi:10.1175/2008JCLI2505.1.

Garfinkel, C. I., D. L. Hartmann, and F. Sassi, 2010: Tropospheric precursors of anomalous Northern Hemisphere stratospheric polar vortices. *J. Climate*, **23**, 3282–3299, doi:10.1175/2010JCLI3010.1.

——, D. W. Waugh, and E. P. Gerber, 2013: The effect of tropospheric jet latitude on coupling between the stratospheric polar vortex and the troposphere. *J. Climate*, **26**, 2077–2095, doi:10.1175/JCLI-D-12-00301.1.

Gerber, E. P., and L. M. Polvani, 2009: Stratosphere–troposphere coupling in a relatively simple AGCM: The importance of stratospheric variability. *J. Climate*, **22**, 1920–1933, doi:10.1175/2008JCLI2548.1.

——, and Coauthors, 2010: Stratosphere-troposphere coupling and annular mode variability in chemistry-climate models. *J. Geophys. Res.*, **115**, D00M06, doi:10.1029/2009JD013770.

Haynes, P. H., M. E. McIntyre, T. G. Shepherd, C. J. Marks, and K. P. Shine, 1991: On the downward control of extratropical diabatic circulations by eddy-induced mean zonal forces. *J. Atmos. Sci.*, **48**, 651–678, doi:10.1175/1520-0469(1991)048<0651:OTCOED>2.0.CO;2.

Held, I. M., and M. J. Suarez, 1994: A proposal for the intercomparison of the dynamical cores of atmospheric general circulation models. *Bull. Amer. Meteor. Soc.*, **75**, 1825–1830, doi:10.1175/1520-0477(1994)075<1825:APFTIO>2.0.CO;2.

Jaiser, R., K. Dethloff, and D. Handorf, 2013: Stratospheric response to Arctic sea ice retreat and associated planetary wave propagation changes. *Tellus*, **65A**, 19375, doi:10.3402/tellusa.v65i0.19375.

Kim, B.-M., S.-W. Son, S.-K. Min, J.-H. Jeong, S.-J. Kim, X. Zhang, T. Shim, and J.-H. Yoon, 2014: Weakening of the stratospheric polar vortex by Arctic sea-ice loss. *Nat. Commun.*, **5**, 4646, doi:10.1038/ncomms5646.

Kushner, P. J., and L. M. Polvani, 2004: Stratosphere–troposphere coupling in a relatively simple AGCM: The role of eddies. *J. Climate*, **17**, 629–639, doi:10.1175/1520-0442(2004)017<0629:SCIARS>2.0.CO;2.

Peings, Y., and G. Magnusdottir, 2014: Response of the wintertime Northern Hemisphere atmospheric circulation to current and projected Arctic sea ice decline: A numerical study with CAM5. *J. Climate*, **27**, 244–264, doi:10.1175/JCLI-D-13-00272.1.

Pithan, F., and T. Mauritsen, 2014: Arctic amplification dominated by temperature feedbacks in contemporary climate models. *Nat. Geosci.*, **7**, 181–184, doi:10.1038/ngeo2071.

Polvani, L. M., and P. J. Kushner, 2002: Tropospheric response to stratospheric perturbations in a relatively simple general circulation model. *Geophys. Res. Lett.*, **29**, 1114, doi:10.1029/2001GL014284.

——, and D. W. Waugh, 2004: Upward wave activity flux as precursor to extreme stratospheric events and subsequent anomalous surface weather regimes. *J. Climate*, **17**, 3548–3554, doi:10.1175/1520-0442(2004)017<3548:UWAFAA>2.0.CO;2.

Scinocca, J. F., M. C. Reader, D. A. Plummer, M. Sigmond, P. J. Kushner, T. G. Shepherd, and A. R. Ravishankara, 2009: Impact of sudden Arctic sea-ice loss on stratospheric polar ozone recovery. *Geophys. Res. Lett.*, **36**, L24701, doi:10.1029/2009GL041239.

Screen, J. A., I. Simmonds, C. Deser, and R. Tomas, 2013: The atmospheric response to three decades of observed Arctic sea ice loss. *J. Climate*, **26**, 1230–1248, doi:10.1175/JCLI-D-12-00063.1.

Simpson, I. R., P. Hitchcock, T. G. Shepherd, and J. F. Scinocca, 2011: Stratospheric variability and tropospheric annular mode timescales. *Geophys. Res. Lett.*, **38**, L20806, doi:10.1029/2011GL049304.

——, ——, ——, and ——, 2013: Southern annular mode dynamics in observations and models. Part I: The influence of climatological zonal wind biases in a comprehensive GCM. *J. Climate*, **26**, 3953–3967, doi:10.1175/JCLI-D-12-00348.1.

Smith, K. L., C. G. Fletcher, and P. J. Kushner, 2010: The role of linear interference in the annular mode response to extratropical surface forcings. *J. Climate*, **23**, 6036–6050, doi:10.1175/2010JCLI3606.1.

Sun, L., C. Deser, L. Polvani, and R. Tomas, 2014: Influence of projected Arctic sea ice loss on polar stratospheric ozone and circulation in spring. *Environ. Res. Lett.*, **9**, 084016, doi:10.1088/1748-9326/9/8/084016.

——, ——, and R. A. Tomas, 2015: Mechanisms of stratospheric and tropospheric circulation response to projected Arctic sea ice loss. *J. Climate*, **28**, 7824–7845, doi:10.1175/JCLI-D-15-0169.1.

Wang, S., E. P. Gerber, and L. M. Polvani, 2012: Abrupt circulation responses to tropical upper-tropospheric warming in a relatively simple stratosphere-resolving AGCM. *J. Climate*, **25**, 4097–4115, doi:10.1175/JCLI-D-11-00166.1.